crystals

MDPI

Article

Comparative Study of Different Crystallization Methods in the Case of Cilostazol Crystal Habit Optimization

Tímea Tari *, Piroska Szabó-Révész and Zoltán Aigner

Institute of Pharmaceutical Technology and Regulatory Affairs, Faculty of Pharmacy, University of Szeged, Eötvös Str. 6, H-6720 Szeged, Hungary; revesz@pharm.u-szeged.hu (P.S.-R.); aigner@pharm.u-szeged.hu (Z.A.)
* Correspondence: tari.timea@pharm.u-szeged.hu; Tel.: +36-1-505-7771

Received: 10 May 2019; Accepted: 4 June 2019; Published: 5 June 2019

Abstract: The therapeutic usage of cilostazol is limited owing to its poor aqueous solubility and oral bioavailability. Our aim was to produce cilostazol crystals with small average particle size; besides suitable roundness, narrow particle size distribution and stable polymorphic form to increase its dissolution rate and improve processability. Different conventional crystallization methods with or without sonication were compared with impinging jet crystallization combined with cooling, and the optimization of the various parameters was also implemented. The effects of post-mixing time and temperature difference were studied by means of a full factorial design. The physical properties of powder particles were characterized by, i.a., XRPD, DSC and SEM. The dissolution rate and the contact angle of solid surfaces were also determined to elucidate the relationship between wettability and dissolution. It was observed that impinging jet crystallization combined with cooling is a very effective and reproducible method for reducing the particle size of cilostazol. This method resulted in significantly smaller particle size (d(0.5) = 3–5 μm) and more uniform crystals compared to the original ground material (d(0.5) = 24 μm) or the conventional methods (d(0.5) = 8–14 μm), and it also resulted in a stable polymorphic form and enhanced the dissolution rate.

Keywords: crystal habit; particle size reduction; cilostazol; impinging jet crystallization; dissolution rate; polymorphism

1. Introduction

During the past decades the number of poorly water-soluble drug candidates has increased extraordinarily in pharmaceutical research and development. In the case of these drugs, new approaches and developments have become necessary to solve poor solubility, low dissolution and oral bioavailability problems. For example, cyclodextrin complexation, co-crystallization, solid dispersion preparation, the use of different salt forms, additives, co-solvents, solubilizing agents or micronization are widespread methods in the pharmaceutical industry [1–4]. Significant progress is also essential in the control of crystallization processes to improve the crystalline product quality, including particle size distribution (PSD), polymorphic form, morphology, purity, flowability, tap density, compactibility, solubility and dissolution rate [5,6]. Namely, different crystallization techniques could result in agglomerated particles and unstable polymorphic forms, poor flow, needle-like crystals, or the products could contain impurities which can decrease stability and efficacy [7,8]. Therefore, already in the early phase of development, the choice of the most appropriate crystallization method and the optimization of crystallization parameters are crucial to achieving a high quality product [9–11].

Conventional crystallization methods, i.e., antisolvent, reverse antisolvent, and cooling crystallization techniques, are frequently used in pharmaceutical industry. The crystallization conditions, such as

temperature, cooling rate, solvent-antisolvent ratio and quality, active pharmaceutical ingredient (API) concentration, mixing factors, etc., can influence the physicochemical properties of the product [12–14]. However, the conventional route can reduce particle size only within certain limits. Therefore, several alternative processes have been developed for the control and modification of the solid-state properties of APIs. For example, laminar-flow tubular crystallizer was used to produce selectively the desired polymorphic form of brivaracetam [15], multi-inlet vortex mixer was redesigned to facilitate formulation screening in small-scale experiments with biologics [16], or continuous plug flow crystallization was applied to generate particles with controlled characteristics [17]. Based on the literature, ultrasound application in crystallization is suitable for modifying the quality of the crystals. It can reduce the metastable zone width, and generate rapid, uniform mixing, which reduces the agglomeration of particles [18,19]. Higher sonication intensity and longer sonication time favour the formation of smaller crystals with narrow PSD [20–22].

Impinging jet crystallization is a relatively new field for the researchers in pharmaceutical manufacturing and industrial crystallization [23]. However, it is proved that this method effectively reduces particle size, as well as it has the potential advantage to produce reproducible products with small average particle size and narrow PSD [24]. The rich solution of the API and the antisolvent flow through two jet nozzles, which are arranged diametrically opposite each other, and it enables the generation of high-intensity micromixing of fluids to achieve high and continual supersaturation before the onset of nucleation at the impinging point [25,26]. Some recent literature developed the impinging jet method with different processes, such as combined with the use of additives to improve the crystal roundness of the products [27] or supplemented with cooling crystallization to narrow crystal size distribution [28].

In the case of poorly water-soluble drugs, which belong to Biopharmaceutics Classification System (BCS) Classes II or IV, the crystal habit is particularly important [29,30]. The small particle size of the final crystallized product can increase dissolution rate and quantity from dosage forms, improve the bioavailability of the drug products, as well as enhance the stability and the uniformity of the API incorporated in tablets [31,32]. Spherical crystal shape favours flowability and fluency during the tableting processes [33]. The smooth surface decreases the agglomeration propensity of the particles, assures the presence of individual particles, therefore fast filtration is facilitated [34]. Overall, these properties appreciably influence the manufacturability and the processability of the given active agent, whether it is pharmaceutical, cosmetic or food industry [35,36].

Cilostazol, 6-[4-(1-cyclohexyl-1H-tetrazol-5-yl)butoxy]-3,4-dihydro-2(1H)-quinolinone is a phosphodiesterase III inhibitor, which suppresses platelet aggregation and has a direct arterial vasodilator effect [37–39]. It exists in three polymorphic forms in a monotropic system. Form A is thermodynamically the most stable, orthorhombic polymorph, Forms B and C are metastable and can be formed only by heat cycling from Form A [40]. Cilostazol belongs to the BCS Class II group, and accordingly, it is poorly soluble and highly permeable. Due to its limited therapeutic usage, several researchers sought to increase the solubility and oral bioavailability of cilostazol by using various procedures [41–43]. Gouthami et al. [44] established that different solvent-antisolvent compositions influence the crystal habit and methanol-hexane and ethanol-hexane resulted in hexagonal and rod shaped habits. The raw material cilostazol has needle-shaped crystals in general, and currently in commerce its average particle size is between 10 and 15 μm. Kim et al. [45] used supercritical antisolvent (SAS) process to reduce the particle size of cilostazol. Remarkable dissolution rate enhancement was observed due to the increased specific surface area. Jinno et al. [46] applied, among others, different mechanical milling processes, such as hammer-mill and jet-mill technologies. These methods resulted in particles with mean diameters of 13 μm and 2.4 μm, respectively.

In the present work our aim was to produce cilostazol crystals with small average particle size, and narrow PSD, besides suitable roundness and stable polymorphic form to improve their processability. The impinging jet (IJ) method was compared with antisolvent (AS), equipped with ultrasound (AS + US) and reverse antisolvent (REV), equipped with ultrasound (REV + US) crystallization

methods. The effects of various post-mixing times and temperature differences were studied by means of a full factorial design in order to optimize the crystallization conditions to achieve a high quality product.

2. Materials and Methods

2.1. Materials

Cilostazol (CIL) was supplied by Egis Pharmaceuticals Plc.; Figure 1 shows its chemical formula. N,N-dimethylformamide (DMF, Scharlau, Barcelona, Spain) was used as solvent and purified water (Ph. Eur. quality) was the antisolvent. Simulated gastric fluid (SGF) without enzymes (10.0 g NaCl, ~59.4 g 37% HCl ad 5000 mL purified water, pH = 1.2 ± 0.1) was used during dissolution investigations.

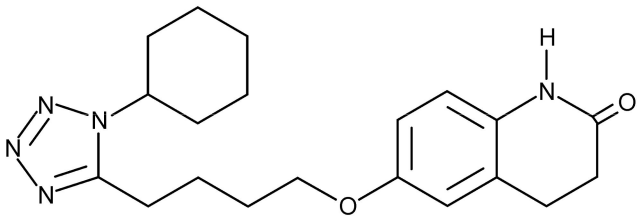

Figure 1. Chemical formula of cilostazol.

2.2. Crystallization Methods

2.2.1. Conventional Crystallization Methods

Conventional crystallization methods were implemented in a 250 mL flat-bottomed, double-walled Schmizo crystallization reactor with constant room temperature provided by the Julabo F32 (Julabo GmbH, Seelbach, Germany) cryothermostat controlled by the Julabo EasyTemp 2.3e software. On-going mixing was carried out with a magnetic stirrer by using an egg-shaped magnetic stir bar. The concentration of the saturated cilostazol solution was 0.0947 g ml^{-1} according to its solubility at 25 °C, and 2 mL of DMF was added to the saturated solution directly before crystallization in order to avoid crystallization in the nozzles. Solubility of cilostazol was practically zero in pure water, furthermore lower temperature resulted in even lower solubility in the same water-DMF mixture. A 1:2 solvent–antisolvent ratio was applied with the volumes of 50 mL near-saturated solution and 100 mL antisolvent. After the precipitation of the product, the filtration was accomplished by a porcelain filter, and the sample was flushed with 40 mL of purified water to minimize the quantity of residual solvent. The products were vacuum dried at 40 °C for 24 hours, then they were stored in closed containers under normal conditions. In the case of the antisolvent system, supersaturation was achieved by exposing the saturated API solution to the antisolvent at 25 °C with fast addition (24 mL min^{-1}) by means of a peristaltic pump. Reverse addition of the solutions was applied in the case of reverse antisolvent crystallization, thus the saturated product solution was added to the antisolvent with 24 mL min^{-1} constant velocity at 25 °C. In both cases the experiments were accomplished with and without the use of high power ultrasound device (Hielscher UP 200S Ultrasonic Processor, Germany). The ultrasound parameters were optimized in previous examinations, ultrasound pulses were set to 0.30 s separated by a gap of 0.70 s, and the amplitude was 70% for both methods.

2.2.2. Impinging Jet Crystallization

Two calibrated peristaltic pumps (Rollpump Type 5198, MTA Kutesz, Budapest, Hungary) fed the near-saturated solution of CIL and the antisolvent to the self-equipped impinging jet unit, which included 0.6-mm-diameter nozzles with the distance of 10 mm, and was arranged in a non-submerged mode. Crystallization experiments were carried out in a 250 mL round-bottomed, double-walled Schmizo crystallization reactor (Schmizo AG, Oftringen, Switzerland). Stirring was accomplished

with an IKA Eurostar digital overhead stirrer (IKA-Werke GmbH & Co., Staufen, Germany) and an Anker-type mixer. Constant temperature was provided by a Thermo Haake P5/C10 (Thermo Haake, Karlsruhe, Germany) thermostat and a Julabo F32 (Julabo GmbH, Seelbach, Germany) cryothermostat controlled by the Julabo EasyTemp 2.3e software. After the preparation of saturated CIL solution, further 2 mL of DMF was added consequently to avoid clogging in the nozzles. The feeding was accomplished with constant linear velocity (4.06 m s^{-1}), which corresponds to the flow rate of 69 mL min^{-1} and with 1:2 solvent–antisolvent ratio, where 50 mL API solution was impinged with 50 mL antisolvent, and further 50 mL antisolvent was in the crystallization reactor, thus the whole crystallization volume was 150 mL. Various temperature differences were adjusted between the solutions: The API solution was kept at 25 °C and the temperature of the antisolvent was modified to 25, 15, or 5 °C. The stirring speed was 250 rpm. The filtration, washing parameters and the storage conditions were the same as at the conventional methods. The schematic drawing of the experimental apparatus is outlined in Figure 2.

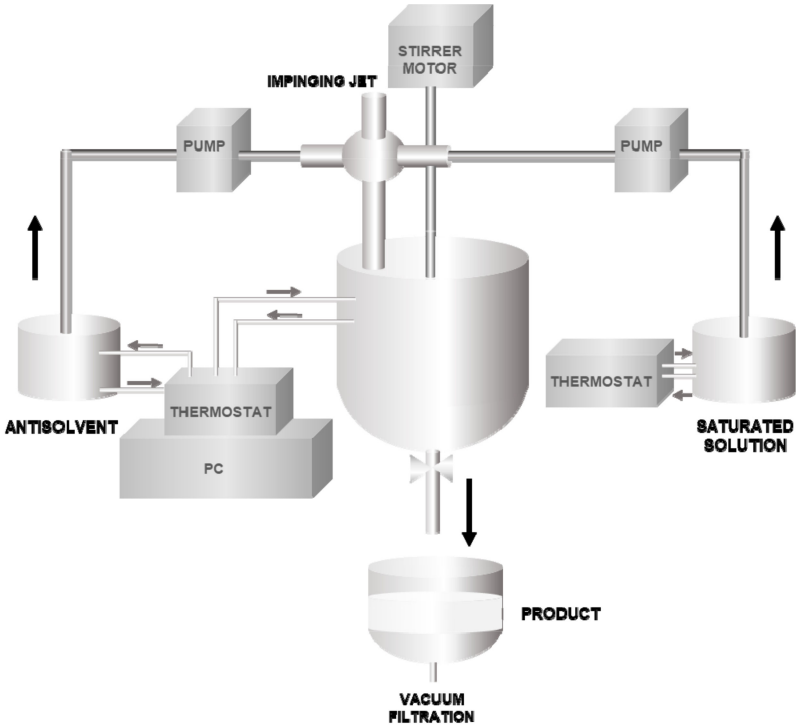

Figure 2. Experimental apparatus of impinging jet crystallization.

2.3. Characterization of the Cilostazol Particles

2.3.1. Determination of Crystal Morphology

Scanning electron microscopy (SEM) (Hitachi S-4700, Hitachi Scientific Ltd., Tokyo, Japan) was applied to examine the morphology of the crystallized products. The working distance was 15 mm with an accelerating voltage of 10 kV and an emission current of 10 mA. A sputter coating apparatus (Bio-Rad SC 502, VG Microtech, Uckfield, UK) was applied to induce electric conductivity on the surface of the samples applying a gold-palladium coating. The argon gas pressure was between 1.3 and 13.0 mPa for 90 s.

The crystal shape of the particles was analyzed by Leica Image Processing and Analysis System (Leica Q 500 MC, Leica Cambridge Ltd., Cambridge, UK) in terms of crystal length, perimeter and roundness for approximately 1000 particles per sample. Roundness is a shape factor, which affords a minimum value of unity for the circle shape, and it is calculated as the ratio of the perimeter squared and the surface area. The adjustment factor of 1.064 corrects the perimeter for the effect of the corners produced by the digitization of the image, which value is a given parameter by the maintenance of the

equipment. The roundness value for the perfect sphere shape equals 1.00. The Leica Image Processing and Analysis System applies the following equation for the determination of roundness:

$$\text{Roundness} = \text{Perimeter}^2/(4\pi \text{ Area } 1.064) \quad (1)$$

2.3.2. Particle Size Distribution Analysis

Malvern Mastersizer laser diffraction analyser (Malvern Instruments Ltd., Malvern, UK) with wet analysis using the Hydro S dispersion unit was applied for PSD analysis, where the defined measuring range was between 0.02 and 2000 μm. The samples were dispersed in purified water with a brief period (3 min) of sonication, and 0.02 mL Polysorbate 80 (VWR International Ltd., Debrecen, Hungary) was added to the solution in order to avoid the aggregation of the particles. The tables with the results contain the mean values and standard deviations of two repeated measurements on each sample, d(0.5) is with a diameter where half of the population lies below, and D[4,3], the mean diameter over the volume.

2.3.3. Identification of Polymorphism

Crystal structure of the samples was analyzed by X-ray powder diffractometry (XRPD) with a Bruker D8 Advance diffractometer (Bruker AXS GmbH, Karlsruhe, Germany). Scattered intensities were measured with a Våntec-1 line detector, symmetrical reflection mode with Cu Ka radiation (λ = 1.5406 Å), and Göbel Mirror bent gradient multilayer optics were used. Relevant measurement conditions were as follows: angular range, from 3° to 40° in steps of 0.01°; target, Cu; filter, Ni; voltage, 40 kV; current, 40 mA; measuring time, 0.1 s/steps. The diffraction patterns of the crystallized samples were compared with those of the structures available in the Cambridge Structural Database (Cambridge Crystallographic Data Centre, CCDC, Cambridge, UK).

A Mettler Toledo differential scanning calorimetry (DSC) 821^e thermal analysis system was applied for the determination of the polymorphism of the samples. 2–5 mg sample was weighed into a 40-μL aluminium crucible, sealed by a lid with three leaks. The linear heating rate was 10 °C min^{-1}, with a temperature interval between 25 and 300 °C, and argon was used as carrier gas with the rate of 100 mL min^{-1}.

2.4. Determination of Wettability by Contact Angle Measurement

Contact angle measurements were conducted under ambient conditions with a DataPhysics Contact Angle System OCA 20 (DataPhysics Instruments, Filderstadt, Germany). CIL compacted pastilles were produced with a manual hydraulic press (Specac Ltd., Orpington, UK). 150 mg CIL powder without any excipient was filled into the 13-mm die and compressed to tablets at a compression force of 0.5 tonnes with a dwell time of 30 s. The sessile drop method was used to determine the contact angle: 5.2 μl of purified water was placed on a compact. The contact angle was measured immediately after the drop reached a quasiequilibrium shape. Triplicate determinations were carried out for each compact.

2.5. Investigation of Dissolution Rate

The dissolution rate of the samples was examined by a European Pharmacopoeia (Ph. Eur. 9th Edition) dissolution apparatus with a modified paddle method (PharmaTest Type PTW II, PharmaTest Apparatebau AG, Hainburg, Germany), using 11.11 mg of pure CIL powder, which corresponds to the dose on the market proportioned in the 100 mL of SGF at a pH value of 1.2 ± 0.1. The suspension was agitated at 100 rpm and sampling was performed up to 120 min (sample volume 5.0 mL). Aliquots were withdrawn at 5, 10, 15, 30, 60, 90, and 120 min, and immediately filtered through 0.2-μm cellulose filters (Phenomenex Syringe filters). At each sampling time, an equal volume of fresh medium was added, and the correction for the cumulative dilution was calculated. Each experiment was run in triplicate. After

filtration and dilution, the CIL contents of the samples were determined UV-spectrophotometrically (λ_{SGF} = 260 nm).

2.6. Statistical Analysis

The impinging jet experiments were laid out by a 3^2 full factorial design to identify the relevant factors which affect the solid state properties of the crystallized product. Calculations were implemented by Statistica for Windows 12 AGA software (StatSoft Inc., Tulsa, OK, USA) with the confidence interval of 95%, i.e. the differences were regarded as significant at $p < 0.05$.

The influence of temperature difference between solutions and post-mixing time on five independent variables, namely on roundness, d(0.5), D[4,3], percentage yield and dissolution rate was investigated. The experiments were performed in a randomized sequence. The following equation describes the interactions of the factors, which was applied to determine the response surface and the relative effects of each factor investigated (b):

$$y = b_0 + b_1x_1 + b_2x_2 + b_3{x_1}^2 + b_4{x_2}^2 + b_5x_1x_2 \quad (2)$$

GraphPad Prism 5 Portable statistical software (GraphPad Software Inc., La Jolla, CA, USA) was applied for the determination of significant differences between the conventional and the impinging jet methods in terms of the mean particle size (d(0.5)) by means of an unpaired t-test.

3. Results and Discussions

3.1. Crystal Morphology

The results of the conventional crystallizations and the data of original grounded material are summarized in Table 1, which present the average values and standard deviations (SD) of the percentage yield, the roundness, and the particle size (d(0.5) and D[4,3]) of the products.

Table 1. Crystallization results of conventional crystallization samples.

Sample Code	US Amplitude	US Cycle Time	Percentage Yield		Roundness		Particle Size			
	(%)	(s)	Mean (m%)	SD	Mean	SD	d(0.5) (μm)	SD	D[4,3] (μm)	SD
AS	0	0.0	88.70	5.35	4.39	0.37	14.411	1.761	19.218	1.268
AS+US	70	0.3	90.39	3.22	2.95	0.19	11.246	1.025	15.738	1.149
REV	0	0.0	55.97	6.70	2.36	0.23	9.906	0.309	12.802	0.521
REV+US	70	0.3	92.93	1.03	2.27	0.27	8.028	0.567	12.006	3.115
Original	-	-	-	-	2.08	0.86	23.563	4.158	60.639	10.294

In the case of the conventional antisolvent crystallization method, the antisolvent was added with the flow rate of 24 mL min^{-1} to the saturated CIL solution, as the fast rate can develop a high degree of supersaturation and lead to smaller particle size. Reverse antisolvent crystallization, where the saturated solution was added to the antisolvent, resulted in smaller particles and more favourable roundness compared to the normal addition. However, the roundness values deteriorated compared to the original material, especially in the case of AS product this value was very high.

The processes were implemented with the application of ultrasound under the same crystallization conditions. It can be established that ultrasound influenced the crystal habit favourably in both cases. Among the conventional processes, reverse antisolvent crystallization equipped with ultrasound resulted in the most appropriate crystal habit.

Table 2 shows the impinging jet crystallization results, where the average particle size of CIL based on the values of d(0.5) was between 3.6 and 4.8 μm. The increase in post-mixing time made the particle size systematically larger, as well as improved percentage yield, but did not affect roundness

appreciably. Due to the lack of post-mixing and immediate filtration, the nuclei had no time to grow further, but the solution could not reach equilibrium, therefore a small amount of API remained dissolved in the solution, and a decline of the percentage yield was experienced.

Table 2. Crystallization results of impinging jet samples.

Sample Code	ΔT	Post Mixing Time	Percentage Yield		Roundness		Particle Size			
	(°C)	(min)	Mean (m%)	SD	Mean	SD	d(0.5) (μm)	SD	D[4,3] (μm)	SD
IJ CIL 1	0	0	79.62	1.21	1.56	0.11	3.887	0.032	5.281	0.046
IJ CIL 2	0	5	81.94	0.95	1.57	0.08	4.259	0.095	5.653	0.084
IJ CIL 3	0	10	87.01	3.58	1.58	0.10	4.801	0.099	6.027	0.077
IJ CIL 4	10	0	79.41	2.70	1.63	0.03	3.810	0.027	5.171	0.029
IJ CIL 5	10	5	85.53	0.82	1.67	0.05	4.134	0.025	5.423	0.057
IJ CIL 6	10	10	86.80	0.29	1.71	0.02	4.557	0.106	6.578	0.091
IJ CIL 7	**20**	**0**	**75.40**	**2.30**	**1.53**	**0.02**	**3.626**	**0.054**	**5.158**	**0.028**
IJ CIL 8	20	5	84.05	0.23	1.66	0.05	3.714	0.019	5.200	0.011
IJ CIL 9	20	10	83.63	0.17	1.63	0.07	3.759	0.018	4.824	0.122

The higher temperature differences between the saturated API solution and the antisolvent decreased the particle size. Since the solubility of CIL depends on temperature, the lower temperature of the antisolvent resulted in even lower solubility and a higher supersaturation value in the same water-DMF mixture and it favoured the producing of smaller particles.

The roundness of the particles was between the values 1.53 and 1.71, which values were independent of the investigated ranges of the parameters; however, roundness improved remarkably compared to the original material and the conventional methods.

If each of the investigated parameters is taken into account, it was found that the most appropriate crystallization condition was when the temperature difference was 20 °C; accordingly, the API solution remained at 25 °C and the antisolvent was cooled down to 5 °C, and the experiments were carried out without post-mixing and filtered immediately after the impingement (IJ CIL 7 product).

All of the crystallized products were filtered easily as the arising filter cake did not cause obstruction in our laboratory-scale experiment, thus the removal of the dispersion medium was satisfactory in all cases.

Overall, it can be stated that the impinging jet method resulted in three-times smaller average particle size and improved roundness appreciably compared with the original grounded material and conventional methods, despite the common application of ultrasound.

In Figure 3 the PSD diagrams of the samples of conventional methods, and the most favourable samples of impinging jet were illustrated and compared to each other. Dry analysis of the samples was not feasible, as the conventionally crystallized samples exhibited a slight tendency to aggregate during these dry circumstances. However, the above described sample preparation procedure ensured the occurrence of individual particles during wet analysis, and all of the crystallized samples were analyzed by the same process conditions in order to the data could be comparable.

Differences in particle size between the samples produced by different procedures can be seen in the diagrams. In the case of conventional methods the effect of ultrasound is obviously noticeable in the curves, the application of ultrasound reduced particle size appreciably in the case of both methods (AS and REV), but they had a wide size distribution and the size reduction did not reach the level of the impinging jet method. The original material and the product of reverse antisolvent combined with ultrasound showed polydisperse distribution, which could be the result of the short sonication duration, combined with the fast addition of the API solution. In contrast, the impinging jet products show smaller particle size, and all of the impinging jet samples revealed monodisperse PSD.

The SEM images represent the disparities in the appearance and morphology of the obtained crystals produced by different crystallization methods. Figure 4 represents the products of conventional crystallization methods, and Figure 5 presents the original material and those impinging jet products

which have the most favourable habit according to the roundness and particle size data given by the Leica Image Processing and Analysis System.

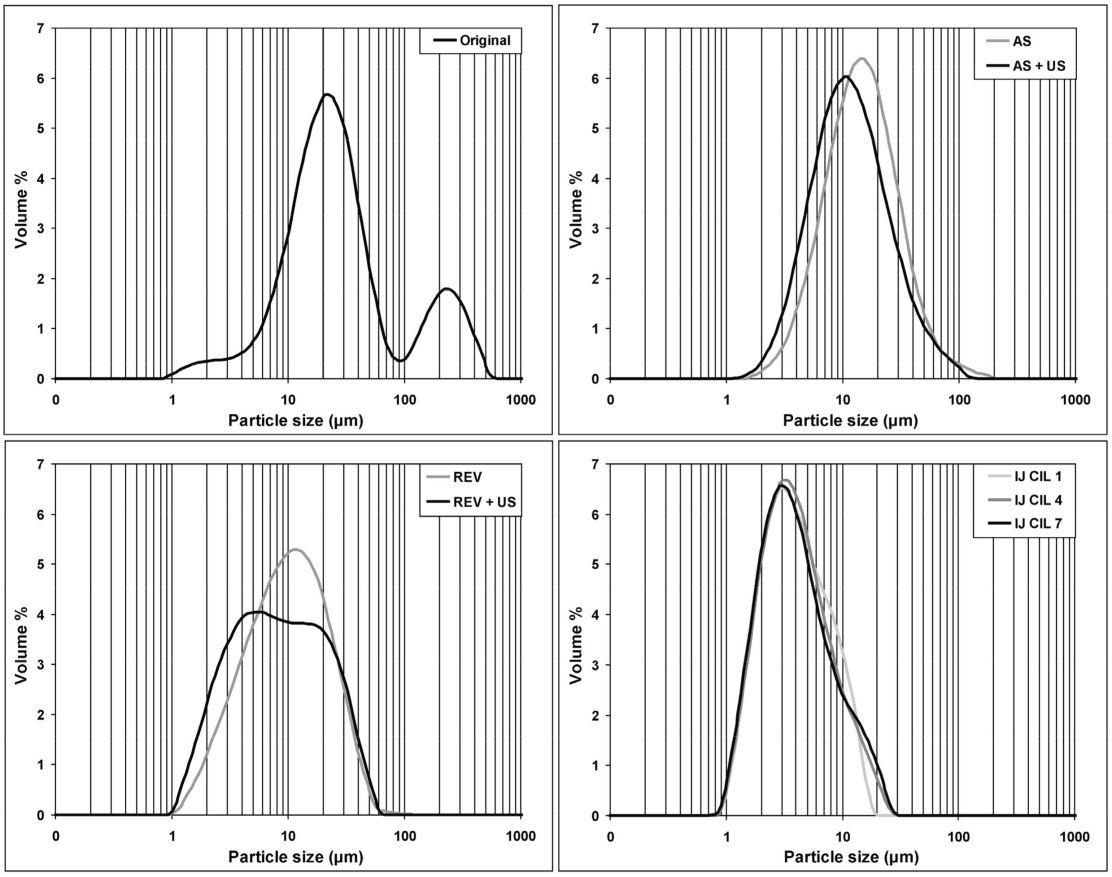

Figure 3. Comparison of particle size distributions of samples made with different crystallization methods.

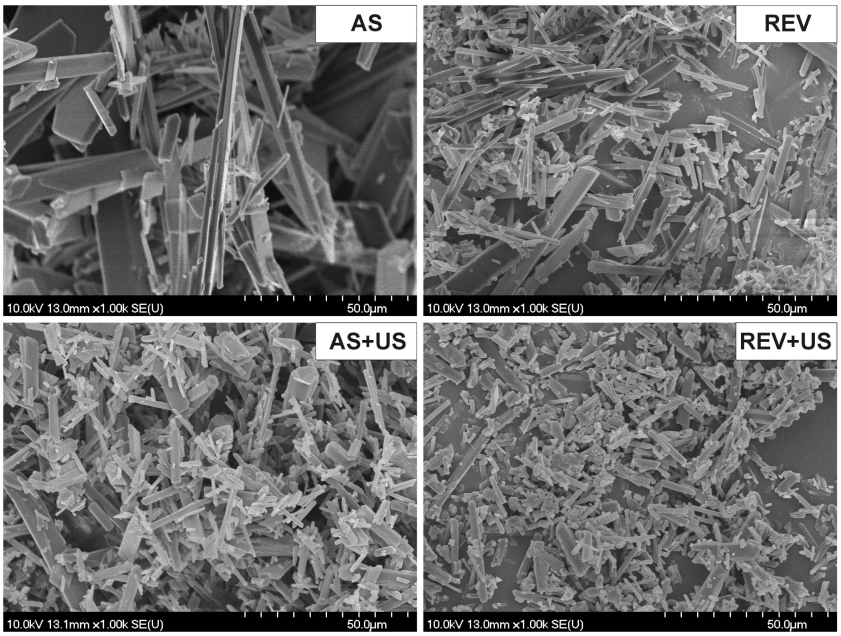

Figure 4. SEM images of the conventional crystallization products.

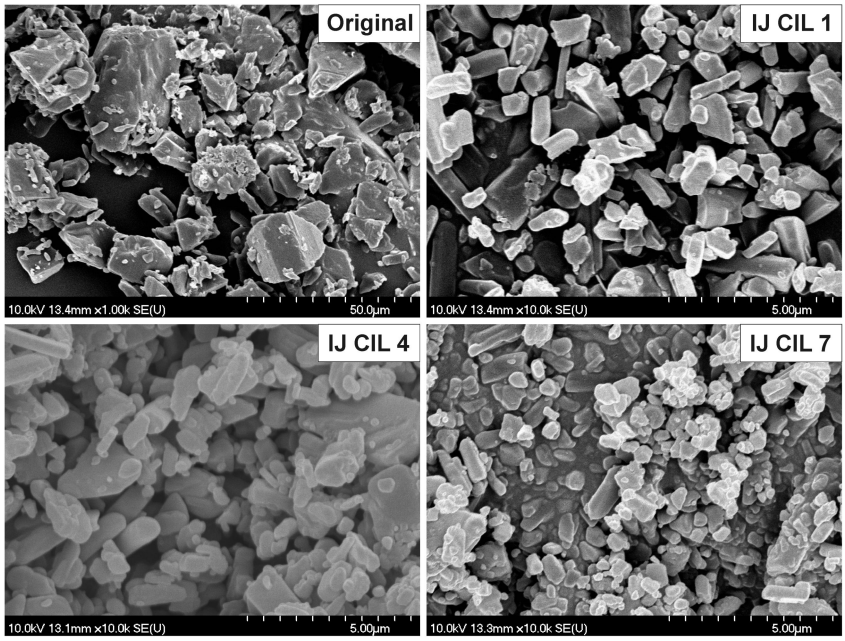

Figure 5. SEM images of original cilostazol crystals and the products made with impinging jet crystallization.

Based on visual observations the conventional crystallization products consisted of bigger-sized and needle-like crystals. The particle size reduction effect of ultrasound is obviously noticeable in the figures as well. The impinging jet products show smooth surface, rounded crystal shape and uniform, individual, small crystals. The original CIL contained large, fragmented crystals with an irregular shape, and small pieces of crystal debris can be considerable, which suggests that the sample was ground in advance. Overall, according to the SEM images the products of impinging jet show the most favourable size and shape, confirming the PSD analysis data.

3.2. Polymorphism

The polymorphism of all of the crystallized products and the initial material were analyzed with XRPD and DSC apparatus in parallel. The Cambridge Structural Database (CSD) diffractograms were compared with the XRPD diffractograms of our products (see Figure 6).

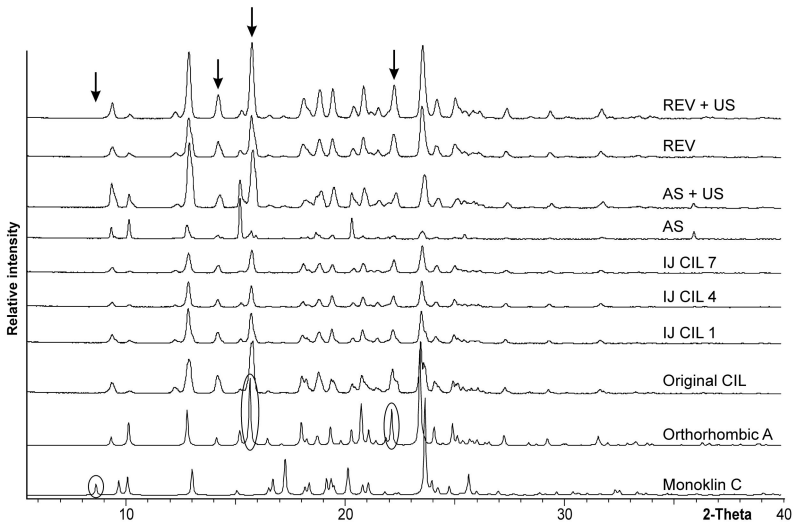

Figure 6. XRPD diffractograms of the crystallized products.

The characteristic peaks of the two polymorphic forms were circled on the CSD diffractograms, and their presence or absence were denoted by arrows on the product diffractograms. Differences were observed between the CSD and our products' diffractograms in terms of the intensity or the breadth of the peaks, but these minor differences might have appeared on account of the habit variations of the different crystallization methods, and the 2-theta values of the peaks are well-comparable. On the diffractograms of the products at 12.161 2-theta value a low peak can be observed, which peak also occurs on the CSD diffractograms of Form A; however, because of the reduction in size of the curve it is not visible sufficiently in the figure. At about 19 and 20 2-theta values, the peaks of the products have inversed intensity compared to the CSD data, which phenomenon can be observed in the initial material as well. On the whole, based on the XRPD analysis, during our experiments no polymorphic transition was observed as compared with the initial material.

The DSC measurements confirmed the XRPD results (see Figure 7). The thermograms of the original CIL and the products also contained one endothermic peak at about 159 °C. Based on the literature, this peak corresponds to the melting point of the Form A polymorphic form, as the Form B and C have the melting points at 136 °C and 146 °C, respectively [40]. Our results indicate that our samples did not contain any of the B- or C-forms, supporting that the crystallization methods applied did not change the polymorph, and the initial stable orthorhombic form was preserved in all the crystallized products. Moreover, the DSC results strengthen the statement that the crystallized products contain pure crystalline material, free from amorphous form.

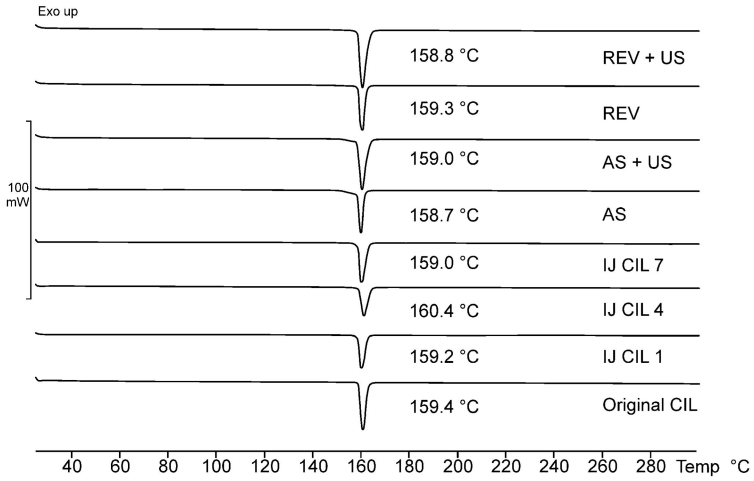

Figure 7. DSC thermograms of the crystallized products.

3.3. Wettability

Wetting is the first step for a solid oral system to dissolve; in addition, it can influence the disintegration time in the medium. Wettability describes the spreading of a liquid on a surface, which is usually indicated by contact angle. The limits of contact angle are 0° for complete wetting and 180° for no wetting [47,48]. Based on our results, which can be seen in Table 3 the impinging jet products' contact angle was lower compared to the products made with conventional methods, which could be correlated with higher solubility values. The smaller particle size resulted in lower contact angle values in every case at 5 s, with the standard deviation of the values set to a constant minimum, which corresponds to the higher wettability.

In the case of the impinging jet products, their uniform surface morphology and small particle size with large surface area influenced advantageously the wettability, which could have a preferential effect on the dissolution rate results as well.

Table 3. Contact angle of the crystallized products measured at 5 s, when the values of SD was set to a constant minimum.

	Original	AS	AS + US	REV	REV + US	IJ CIL 1	IJ CIL 4	IJ CIL 7
Mean (°)	62.4	61.7	59.9	58.5	54.6	52.1	53.3	46.9
SD	1.3	1.1	0.6	1.1	0.9	0.4	0.2	0.2

3.4. Dissolution Rate

The dissolution profile of the pure CIL products was accomplished by 120-min-range in vitro studies in SGF without enzymes (pH = 1.2 ± 0.1). The dissolution curves are presented in Figure 8 to illustrate the effects of different crystallization methods. After 5 min, the ratio of dissolved CIL ranged between 0.03 and 0.53 mg 100 mL^{-1}, depending on the crystallization method. The wide range shows the strong influence of particle sizes on the responses. On the dissolution curve at 5 min, a rapid increase of dissolution can be observed in the case of IJ CIL 7 sample, which is a typical phenomenon when small particles possess a large surface area, while in the case of the conventional products, the aggregated, needle-like, and bigger crystals delayed dissolution. Remarkable differences can be observed at 10 min of the dissolution rates, as IJ CIL 7 sample reached the 0.68 mg 100 mL^{-1} value at 10 min, while IJ CIL 1 and 4 samples at 30 min, REV samples at 60 min, and AS samples only at 120 min achieved that value. Among the conventional processes, the reverse antisolvent crystallization equipped with ultrasound increased the dissolution rate to the highest degree. At 120 min, the IJ CIL 7 sample resulted in higher dissolution quantity compared with the conventional samples.

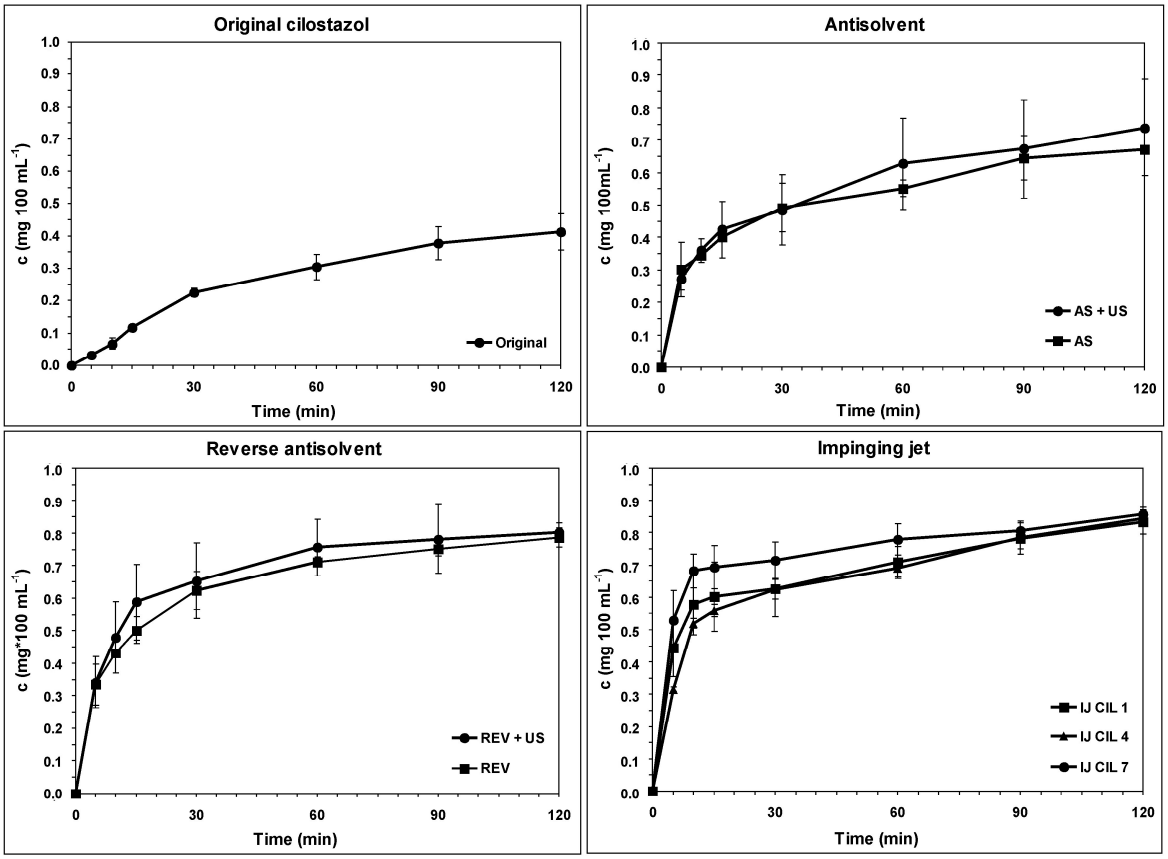

Figure 8. Dissolution rate of the crystallized products.

On the one hand, as the error bars of the values are overlapped in some cases through the measured period, significance between the IJ samples and the conventional method samples could not be firmly stated in terms of dissolution rate. On the other hand, at particular initial points of the process a clear

correlation is revealed between the dissolution rate and the particle size; the smaller size improved the dissolution rate. If the unique, small particles could remain in the final dosage form as well, the higher dissolved concentration of the API in the initial period of dissolution could improve bioavailability.

3.5. Statistical Analysis

The purpose of the statistical analysis was to explore the effects of the impinging jet crystallization parameters on particle size, roundness, percentage yield and dissolution rate, on the one hand. In Table 4 the significant factors were underlined. The results demonstrates that both temperature difference and post-mixing time revealed significant, linear effect on particle size (d(0.5)), while they had no significant effects on roundness because of outlier data. As for dissolution rate, the temperature difference verified a quadratic significant effect, when the difference is higher, it enhances dissolution. Post-mixing time was found to have a significant relationship with the changes of percentage yield values. Thus, increasing post-mixing time was proved to improve yield. Based on these results, the most favourable set concerning the crystal habit was the 20 °C temperature difference with 0 min post-mixing. For all significant effects $p < 0.038$.

Table 4. Statistical analysis results of the factorial design. (x_1: Post-mixing time; x_2: Temperature difference).

Dependent Variable	Polynomial Function	r^2
d(0.5)	$y = 4.06 + \mathbf{0.30x_1 - 0.31x_2} - 0.02x_1^2 + 0.08x_2^2 - 0.20x_1x_2$	0.870
D[4,3]	$y = 5.48 + 0.30x_1 - 0.30x_2 - 0.04x_1^2 + 0.18x_2^2 - 0.27x_1x_2$	0.596
Roundness	$y = 1.2 - 0.02x_1 - 0.002x_2 + 0.01x_1^2 + 0.03x_2^2 - 0.01x_1x_2$	0.401
Dissolution rate	$y = 7.38 - 0.09x_1 + 0.16x_2 + 0.09x_1^2 \mathbf{- 0.22x_2^2} - 0.04x_1x_2$	0.797
Percentage yield	$y = 82.60 \mathbf{+ 3.84x_1} - 0.92x_2 + 0.93x_1^2 - 0.99x_2^2 + 0.21x_1x_2$	0.899

On the other hand, each of the conventional methods was compared with the impinging jet results in terms of particle size (d(0.5)). Figure 9 presents the level of significance between the different methods. Based on the unpaired t-test, the impinging jet method resulted in a significantly smaller particle size ($p < 0.04$) in every case. The significant effect of ultrasound is also considerable, the application of sonication advanced particle size reduction, not only in antisolvent, but also in reverse antisolvent crystallization ($p < 0.05$).

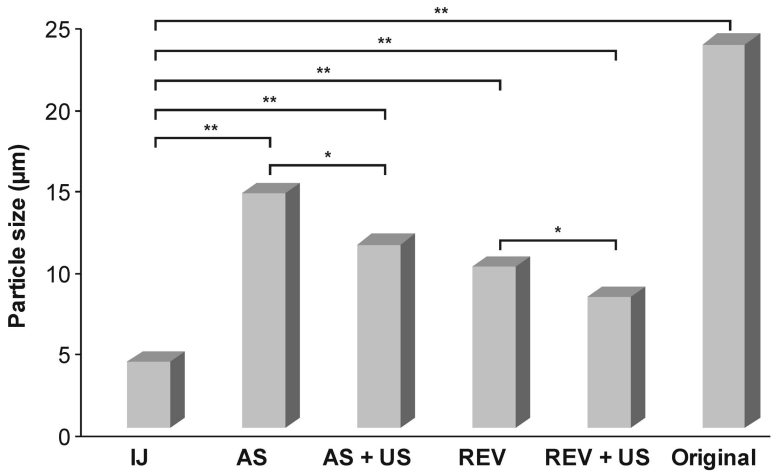

Figure 9. Statistical comparison of the particle size (d(0.5)) of the crystallized products. Significance level: * $p < 0.05$; ** $p < 0.01$.

4. Conclusions

It was observed that the self-equipped impinging jet apparatus is a very effective and reproducible method for reducing the particle size of cilostazol. Post-mixing time and temperature difference are

the significant factors in the case of particle size modification. The particle size distribution was monodisperse, and the average particle size was significantly smaller (d(0.5) = 3.62–4.80 μm) and more uniform compared to the original ground material (d(0.5) = 23.57 μm), as well as compared to the traditional crystallization methods, even with the application of ultrasound (d(0.5) = 8.03–14.41 μm). This method resulted in stable orthorhombic polymorphic form (Form A); thus, it can be stated that the morphology of the crystals was modified in consequence of the crystallization conditions, and it was not the characteristic of another polymorphic form. Impinging jet product with optimal adjusted crystallization parameters enhanced the dissolution rate in contrast to the products of conventional crystallization methods and the original ground material. Therefore, the combined cooling and impinging jet method is a promising approach to optimizing the crystal habit and to practical application in the manufacture of cilostazol. The observations about the crucial process parameters can serve as a basis for the crystal habit optimization of other poorly water-soluble substances as well. If a certain crystal habit is preferred, changing the crystallization method itself might be sufficient to achieve morphology modification without polymorphic transition, and further alterations, such as solvent exchange, using additives, or other excipients would not be necessary any more. The comparison of the different conventional crystallization methods revealed their particle size reduction capacity, and the results can ease the decision on which method is suitable for attaining the desired particle size range.

Author Contributions: T.T. and Z.A. conceived the research and designed the experiments. Formal analysis, investigation, data curation, T.T.; writing—original draft preparation, T.T., Z.A.; writing—review and editing, T.T., Z.A., P.S.-R.; supervision Z.A., P.S.-R.

Funding: This research received no external funding.

Acknowledgments: The authors are grateful to Béla Farkas for his contribution and excellent assistance to this project. The authors also would like to thank Rita Ambrus for implementing SEM analysis. API was provided by Egis Pharmaceuticals Plc., Budapest, Hungary.

Conflicts of Interest: The authors declare no conflict of interest.

References

1. Miletic, T.; Kyriakos, K.; Graovac, A.; Ibric, S. Spray-dried voriconazole–cyclodextrin complexes: Solubility, dissolution rate and chemical stability. *Carbohydr. Polym.* **2013**, *98*, 122–131. [CrossRef] [PubMed]
2. Lu, Y.; Tang, N.; Lian, R.; Qi, J.; Wu, W. Understanding the relationship between wettability and dissolution of solid dispersion. *Int. J. Pharm.* **2014**, *465*, 25–31. [CrossRef] [PubMed]
3. Rasenack, N.; Müller, B.W. Micron-size drug particles: Common and novel micronization techniques. *Pharm. Dev. Technol.* **2004**, *9*, 1–13. [CrossRef] [PubMed]
4. Patole, T.; Deshpande, A. Co-crystallization—A technique for solubility enhancement. *Int. J. Pharm. Sci. Res.* **2014**, *5*, 3566–3576.
5. Gao, Z.; Rohani, S.; Gong, J.; Wang, J. Recent developments in the crystallization process: Toward the pharmaceutical industry. *Engineering* **2017**, *3*, 343–353. [CrossRef]
6. Pitt, K.; Peña, R.; Tew, J.D.; Pal, K.; Smith, R.; Nagy, Z.K.; Litster, J.D. Particle design via spherical agglomeration: A critical review of controlling parameters, rate processes and modelling. *Powder Technol.* **2018**, *326*, 327–343. [CrossRef]
7. Lovette, M.A.; Doherty, M.F. Needle-shaped crystals: Causality and solvent selection guidance based on periodic bond chains. *Cryst. Growth Des.* **2013**, *13*, 3341–3352. [CrossRef]
8. Simone, E.; Othman, R.; Vladisavljevic, G.T.; Nagy, K.Z. Preventing crystal agglomeration of pharmaceutical crystals using temperature cycling and a novel membrane crystallization procedure for seed crystal generation. *Pharmaceutics* **2018**, *10*, 17. [CrossRef]
9. Han, X.; Ghoroi, C.; To, D.; Chen, Y.; Davé, R. Simultaneous micronization and surface modification for improvement of flow and dissolution of drug particles. *Int. J. Pharm.* **2011**, *415*, 185–195. [CrossRef]
10. Vandana, K.; Raju, Y.P.; Chowdary, V.H.; Sushma, M.; Kumar, N.V. An overview on in situ micronization technique—An emerging novel concept in advanced drug delivery. *Saudi Pharm. J.* **2014**, *22*, 283–289. [CrossRef]

11. An, J.-H.; Kiyonga, A.N.; Lee, E.H.; Jung, K. Simple and efficient spherical crystallization of clopidogrel bisulfate form-I via anti-solvent crystallization method. *Crystals* **2019**, *9*, 53. [CrossRef]
12. am Ende, D.J.; Brenek, S.J. Strategies to control particle size during crystallization processes. *Am. Pharm. Rev.* **2004**, *7*, 98–104.
13. Aigner, Z.; Szegedi, Á.; Szabadi, V.; Ambrus, R.; Sovány, T.; Szabó-Révész, P. Comparative study of crystallization processes in case of glycine crystallization. *Acta Pharm. Hung.* **2012**, *82*, 61–68. [PubMed]
14. Matsumoto, M.; Wada, Y.; Onoe, K. Change in glycine polymorphs induced by minute-bubble injection during antisolvent crystallization. *Adv. Powder Technol.* **2015**, *26*, 415–421. [CrossRef]
15. Rimez, B.; Debuysschère, R.; Conté, J.; Lecomte-Norrant, E.; Gourdon, C.; Cognet, P.; Scheid, B. Continuous-flow tubular crystallization to discriminate between two competing crystal polymorphs. 1. Cooling crystallization. *Cryst. Growth Des.* **2018**, *18*, 6431–6439. [CrossRef]
16. Chester, E.; Markwalter, C.E.; Prud'homme, R.K. Design of a small-scale multi-inlet vortex mixer for scalable nanoparticle production and application to the encapsulation of biologics by inverse flash nanoprecipitation. *J. Pharm. Sci.* **2018**, *107*, 2465–2471.
17. Alvarez, A.J.; Myerson, A.S. Continuous plug flow crystallization of pharmaceutical compounds. *Cryst. Growth Des.* **2010**, *10*, 2219–2228. [CrossRef]
18. Su, C.-S.; Liao, C.-Y.; Jheng, W.-D. Particle size control and crystal habit modification of phenacetin using ultrasonic crystallization. *Chem. Eng. Technol.* **2015**, *38*, 181–186. [CrossRef]
19. Kim, H.N.; Suslick, K.S. The effects of ultrasound on crystals: Sonocrystallization and sonofragmentation. *Crystals* **2018**, *8*, 280. [CrossRef]
20. Dhumal, R.S.; Biradar, S.V.; Paradkar, A.R.; York, P. Particle engineering using sonocrystallization: Salbutamol sulphate for pulmonary delivery. *Int. J. Pharm.* **2009**, *368*, 129–137. [CrossRef]
21. Gielen, B.; Claes, T.; Janssens, J.; Jordens, J.; Thomassen, L.C.J.; Gerven, T.V.; Braeken, L. Particle size control during ultrasonic cooling crystallization of paracetamol. *Chem. Eng. Technol.* **2017**, *40*, 1300–1308. [CrossRef]
22. Yang, Z.-Y.; Yen, S.-K.; Hu, W.-S.; Huang, Y.-Z.; Yang, T.-M.; Su, C.-S. Sonocrystallization—Case studies of salicylamide particle size reduction and isoniazid derivative synthesis and crystallization. *Crystals* **2018**, *8*, 249. [CrossRef]
23. Cheng, J.; Yang, C.; Jiang, M.; Li, Q.; Mao, Z.-S. Simulation of antisolvent crystallization in impinging jets with coupled multiphase flow-micromixing-PBE. *Chem. Eng. Sci.* **2017**, *171*, 500–512. [CrossRef]
24. Tari, T.; Fekete, Z.; Szabó-Révész, P.; Aigner, Z. Reduction of glycine particle size by impinging jet crystallization. *Int. J. Pharm.* **2015**, *478*, 96–102. [CrossRef] [PubMed]
25. Calvignac, B.; Boutin, O. The impinging jets technology: A contacting device using a SAS process type. *Powder Technol.* **2009**, *191*, 200–205. [CrossRef]
26. Tamura, H.; Kadota, K.; Shirakawa, Y.; Tozuka, Y.; Shimosaka, A.; Hidaka, J. Morphology control of amino acid particles in interfacial crystallization using inkjet nozzle. *Adv. Powder Technol.* **2014**, *25*, 847–852. [CrossRef]
27. Tari, T.; Ambrus, R.; Szakonyi, G.; Madarász, D.; Frohberg, P.; Csóka, I.; Szabó-Révész, P.; Ulrich, J.; Aigner, Z. Optimizing the crystal habit of glycine by using additive for impinging jet crystallization. *Chem. Eng. Technol.* **2017**, *40*, 1323–1331. [CrossRef]
28. Jiang, M.; Li, Y.-E.D.; Tung, H.-H.; Braatz, R.D. Effect of jet velocity on crystal size distribution from antisolvent and cooling crystallizations in a dual impinging jet mixer. *Chem. Eng. Process.* **2015**, *97*, 242–247. [CrossRef]
29. Dubbini, A.; Censi, R.; Martena, V.; Hoti, E.; Ricciutelli, M.; Malaj, L.; Martino, P.D. Influence of pH and method of crystallization on the solid physical form of indomethacin. *Int. J. Pharm.* **2014**, *473*, 536–544. [CrossRef]
30. Blagden, N.; de Matas, M.; Gavan, P.T.; York, P. Crystal engineering of active pharmaceutical ingredients to improve solubility and dissolution rates. *Adv. Drug Deliv. Rev.* **2007**, *59*, 617–630. [CrossRef]
31. Kakran, M.; Sahoo, N.G.; Li, L.; Judeh, Z. Particle size reduction of poorly water soluble artemisinin via antisolvent precipitation with a syringe pump. *Powder Technol.* **2013**, *237*, 468–476. [CrossRef]
32. Xu, J.; Luo, K.Q. Enhancing the solubility and bioavailability of isoflavone by particle size reduction using a supercritical carbondioxide-based precipitation. *Chem. Eng. Res. Des.* **2014**, *92*, 2542–2549. [CrossRef]
33. Szabó-Révész, P.; Göcző, H.; Pintye-Hódi, K.; Kása, P.; Erős, I.; Hasznos-Nezdei, M.; Farkas, B. Development of spherical crystal agglomerates of an aspartic acid salt for direct tablet making. *Powder Technol.* **2011**, *114*, 118–124. [CrossRef]

34. Lin, R.; Liu, W.; Woo, M.W.; Chen, X.D.; Selomulya, C. On the formation of "coral-like" spherical α-glycine crystalline particles. *Powder Technol.* **2015**, *279*, 310–316. [CrossRef]
35. Tanaka, M.; Yamanaka, S.; Shirakawa, Y.; Shimosaka, A.; Hidaka, J. Preparation of porous particles by liquid–liquid interfacial crystallization. *Adv. Powder Technol.* **2011**, *22*, 125–130. [CrossRef]
36. Hesselbach, J.; Barth, N.; Lippe, K.; Schilde, C.; Kwade, A. Process chain and characterisation of nanoparticle enhanced composite coatings. *Adv. Powder Technol.* **2015**, *26*, 1624–1632. [CrossRef]
37. Hayato, U.; Toshio, T.; Yukio, K.; Hiroyoshi, H. Purification of cyclic adenosine monophosphate phosphodiesterase from human platelets using new-inhibitor sepharose chromatography. *Biochem. Pharmacol.* **1984**, *33*, 3339–3344. [CrossRef]
38. Mahmoud, D.B.; Shukr, H.; Bendas, E.R. In vitro and in vivo evaluation of self-nanoemulsifying drug delivery systems of cilostazol for oral and parenteral administration. *Int. J. Pharm.* **2014**, *476*, 60–69. [CrossRef]
39. Ha, E.-S.; Ha, D.-H.; Kuk, D.-H.; Sim, W.-Y.; Baek, I.-H.; Kim, J.-S.; Park, H.J.; Kim, M.-S. Solubility of cilostazol in the presence of polyethylene glycol 4000, polyethylene glycol 6000, polyvinylpyrrolidone K30, and poly(1-vinylpyrrolidone-co-vinyl acetate) at different temperatures. *J. Chem. Thermodyn.* **2017**, *113*, 6–10. [CrossRef]
40. Stowell, G.W.; Behme, R.J.; Denton, S.M.; Pfeiffer, I.; Sancilio, F.D.; Whittall, L.B.; Whittle, R.R. Thermally-prepared polymorphic forms of cilostazol. *J. Pharm. Sci.* **2002**, *91*, 2481–2488. [CrossRef]
41. Mustapha, O.; Kim, K.S.; Shafique, S.; Kim, D.S.; Jin, S.G.; Seo, Y.G.; Youn, Y.S.; Oh, K.T.; Lee, B.J.; Park, Y.J.; et al. Development of novel cilostazol–loaded solid SNEDDS using a SPG membrane emulsification technique: Physicochemical characterization and in vivo evaluation. *Colloids Surf. B* **2017**, *150*, 216–222. [CrossRef] [PubMed]
42. Mustapha, O.; Kim, K.S.; Shafique, S.; Kim, D.S.; Jin, S.G.; Seo, Y.G.; Youn, Y.S.; Oh, K.T.; Yong, C.S.; Kim, J.O.; et al. Comparison of three different types of cilostazol-loaded solid dispersion: Physicochemical characterization and pharmacokinetics in rats. *Colloids Surf. B* **2017**, *154*, 89–95. [CrossRef] [PubMed]
43. Miao, X.; Sun, C.; Jiang, T.; Zheng, L.; Wang, T.; Wang, S. Investigation of nanosized crystalline form to improve the oral bioavailability of poorly water soluble cilostazol. *J. Pharm. Pharm. Sci.* **2011**, *14*, 196–214. [CrossRef] [PubMed]
44. Gouthami, K.S.; Kumar, D.; Thipparaboina, R.; Chavan, R.B.; Shastri, N.R. Can crystal engineering be as beneficial as micronisation and overcome its pitfalls?: A case study with cilostazol. *Int. J. Pharm.* **2015**, *491*, 26–34. [CrossRef] [PubMed]
45. Kim, M.-S.; Lee, S.; Park, J.-S.; Woo, J.-S.; Hwang, S.-J. Micronization of cilostazol using supercritical antisolvent (SAS) process: Effect of process parameters. *Powder Technol.* **2007**, *177*, 64–70. [CrossRef]
46. Jinno, J.-I.; Kamada, N.; Miyake, M.; Yamada, K.; Mukai, T.; Odomi, M.; Toguchi, H.; Liversidge, G.G.; Higaki, K.; Kimura, T. Effect of particle size reduction on dissolution and oral absorption of a poorly water-soluble drug, cilostazol, in beagle dogs. *J. Control. Release* **2006**, *111*, 56–64. [CrossRef]
47. Dahlberg, C.; Millqvist-Fureby, A.; Schuleit, M. Surface composition and contact angle relationships for differently prepared solid dispersions. *Eur. J. Pharm. Biopharm.* **2008**, *70*, 478–485. [CrossRef]
48. Tian, F.; Sandler, N.; Aaltonen, J.; Lang, C.; Saville, D.J.; Gordon, K.C.; Strachan, C.J.; Rantanen, J.; Rades, T. Influence of polymorphic form, morphology, and excipient interactions on the dissolution of carbamazepine compacts. *J. Pharm. Sci.* **2007**, *96*, 584–594. [CrossRef]